Understanding the mechanism of adsorption of CTAB and polylysine on silver nanoparticles and detection of Hg^{2+}: Experimental and DFT study

Lovika Moudgil [a], Jyoti Jaiswal [b], Anu Mittal [c], G.S.S. Saini [a], Gurinder Singh [d], Aman Kaura [d],*

[a] Department of Physics, Centre of Advanced Study in Physics, Panjab University, Chandigarh 160014, India
[b] Institute Instrumentation Centre, Indian Institute of Technology Roorkee, 247667, India
[c] Department of Chemistry, Guru Nanak Dev University College, Chungh, Distt. Tarntaran, India
[d] Department of UIET, Panjab University SSG Regional Centre Hoshiarpur, Panjab 146001, India

ARTICLE INFO

ABSTRACT

Fundamental aspects of poly-L-lysine (PLL) coated silver nanoparticles (AgNPs) are presented for their possible use in colorimetric sensing of heavy metal ions. For this purpose, cetyltrimethylammonium bromide (CTAB) is used, which acts as a stabilizing agent. At the molecular level, the adsorption behavior of PLL and CTAB is evaluated from first principles calculations. These studies demonstrate that PLL and CTAB interact with Ag cluster through NH_2 group and positively charged trimethylammonium group, respectively. Surface adsorption of PLL and CTAB on AgNPs is studied under the effect of temperature and reaction time. Multidisciplinary approaches including UV–Visible absorption spectroscopy, Fourier-Transformed Infrared Spectroscopy (FT-IR), Transmission Electron Microscopy (TEM) are conducted to systematically investigate PLL coated AgNPs stabilized by CTAB (PL-CT-AgNPs). Thus, a combination of experimental and theoretical analysis helped us to identify specific sites, which promoted such interactions for surface adsorption on AgNPs. As synthesized PL-CT-AgNPs, are found to be highly sensitive and selective towards Hg^{2+} detection. The mechanism of detection of Hg^{2+} is studied on PL-CT-AgNPs surface using Density Functional Theory (DFT).

© 2018 Elsevier B.V. All rights reserved.

1. Introduction

Metal nanoparticles particularly silver and gold have received a lot of attention because of their unexampled optical properties [1,2]. They are always preferred because of having distinctive properties like large surface area to volume ratio, stability over high temperature, and small size that allows more points of contacts than that of bulk compound [3]. The AgNPs although being less stable in comparison to gold nanoparticles have higher plasmon excitation efficiency [4]. Amino acids being the building block for polypeptides and proteins are of prime importance for life and help to pay particular attention to countless studies in scientific fields [5–7]. Recently, research has directed attention to the binding of AgNPs with peptides [8,9] The study of peptide on AgNPs surface is an interesting probe molecule because of having variety of functional groups and that can be found in the same molecule (—OH, —COOH, —NH₂, —CHₓ, —SH, —NH₂ etc.). Particularly, functional groups like -SH and -NH₂ have high affinity for Ag, thus they also help to stabilize AgNPs [10]. Similarly, the cationic surfactant CTAB is used as shape directing agent to control the morphology of the AgNPs. A lot of data has been published previously on the synthesis of AgNPs using biomolecules as capping agents in the presence of different surfactants as stabilizer [11–14]. Despite large amount of work done on these materials, an approach in line with theoretical framework is urgently required because the capping agent and stabilizer have number of different modes through which they can interact with the AgNPs. An approach based on the first principles method, not only provide the most favorable interaction site but also the electronic structure factors responsible for it.

A higher concentration of metal ions such as Hg^{2+}, Ni^{2+}, K^+, Pb^{2+}, Co^{2+}, Fe^{3+}, and Cu^{2+} in the water poses a significant hazard to human beings and environment [15]. Mercury is one of the toxic elements to human being. It can affect central and peripheral nervous system. It can lead to neurological and behavioral disorders [16]. The routine laboratory techniques such as atomic absorption spectroscopy [17], atomic fluorescence spectrometry and inductively coupled mass spectroscopies [18,19] are in common use to measure the concentration of different metal ions, but these methods require complex machinery to provide any meaningful measurements. Naked eye detection of metal ions is possible in aqueous medium because of metal nanoparticles. There are reports on heavy metal ion detection using metal NPs [20]. The two mechanisms by which AgNPs senses metal ions in the aqueous medium are mainly by the redox reaction between AgNPs and metal ions or based on the aggregation of AgNPs. Farhadi et al. [21] have synthesized AgNPs in the presence of the manna of hedysarum plant and soap-root plant. The synthesized AgNPs are

* Corresponding author.
  E-mail address: amankaura@pu.ac.in (A. Kaura).

initially yellowish-brown in color due to the presence of Surface Plasmon Resonance (SPR) absorption band. However, when Hg^{2+} ions are added to the solution, then Hg^{2+} formed a bond with the AgNPs surface and dragged the biological stabilizer away from the surface of AgNPs. This resulted in the redox reaction between AgNPs and Hg^{2+} ions.

Wang et al. [22] have developed aggregation based system to detect Hg^{2+} ions. They have considered the adsorption of mercury specific oligonucleotides in random coil form on AgNPs. When Hg^{2+} adsorbs, there is folding of random coil structure and it transforms into rigid stem-loop structure. This rigid structure then prefers to move mercury specific oligonucleotides bases away from AgNPs. This created a region of high negative charges, which increase the repulsion between mercury specific oligonucleotides and AgNPs. This changes the color of solution from yellow to red. Annadhasan et al. [23] synthesized AgNPs in the presence of L-tyrosine and studied the detection of Hg^{2+} and Mn^{2+}. They observed that as the concentration of Hg^{2+} ions is increased, a blue shift is observed. This could be due to the reduction of Hg^{2+} ions. However, interaction of Mn^{2+} ions with AgNPs resulted in the red-shift of SPR band. This is because of the aggregation of AgNPs, which is attributed to the complex formation between L-tyrosine capped AgNPs and Mn^{2+} ions.

In all these studies, a plausible mechanism is explained for interaction of metal ions with capped AgNPs. To the best of our knowledge, theoretical framework for the reduction or aggregation of metal ions with AgNPs is rarely investigated [23,24]. In order to accomplish this task, a combined theoretical and experimental study can provide us guiding rules to fabricate a sensor for the detection of specific analyte.

In this paper, we have investigated the reasons behind the large affinity of the PLL and CTAB with AgNPs with the help of DFT method. We have also reported the DFT studies to explain the mechanism of detection of Hg^{2+} on PL-CT-AgNPs. On the basis of the inference made from theoretical calculations, experimental work has been performed to develop nanosilver-based colorimetric sensor for the detection of Hg^{2+} ions in the aqueous solution. The surface functionalization of AgNPs is carried out in the presence of optimum concentration of polypeptide, PLL (Fig. SI-1a) and an inorganic molecule, CTAB (Fig. SI-1b). PLL coated AgNPs are stabilized by CTAB, which lead to the colorimetric sensing of Hg^{2+}. Thus, this work will pave the way to identify the specific sites on AgNPs surface using a combination of theoretical and experimental analysis upto molecular level and demonstrated their colorimetric applicability.

2. Computational details

As a quantum mechanical method, DFT calculations are considered to be the best way for systematic and precise determination of binding energy, electronic structure of different molecular and atomic structures. We have performed DFT calculations using the 6-31G basis sets for C, H, O, N atoms and LANL2DZ double-split basis set for Ag atoms with B3LYP functional (Becke's 3-parameter exchange functional with Lee-Yang-Parr correlation energy functional) [25]. These basis sets have been used previously in the literature and provide satisfactorily results of different properties [26]. The optimization is considered to be complete when energies and total forces drop below the respective threshold of 10^{-4} au and 10^{-3} au. The minimization is performed with the long range corrected LC-wPBE exchange correlation functional in the atomic orbital based NWCHEM package [27]. Chemissian software [28] package is used for the analysis of resulting orbitals and the electronic composition.

3. Experimental method

Materials: Silver nitrate ($AgNO_3$), PLL, CTAB, $Al(NO_3)_3.9H_2O$, $Cd(NO_3)_2.4H_2O$, $Sr(NO_3)_2$, $Mg(NO_3)_2 \cdot 6H_2O$, $Co(NO_3)_2 \cdot 6H_2O$, $Ni(NO_3)_2 \cdot 6H_2O$, $Ca(Na_3)_2 \cdot 4H_2O$, $Cu(NO_3)_2 \cdot 3H_2O$, $Zn(NO_3)_2 \cdot 6H_2O$, $Hg(NO_3)_2 \cdot H_2O$, $Mn(NO_3)_2$, $Cr(NO_3)_2 \cdot 9H_2O$ are purchased from Sigma Aldrich,

India. Triple distilled water is used for all experiments. Aqua-regia (HCl: HNO_3 = 3:1 (v/v)) is used for washing glass wares and further washed with triple distilled water before use.

3.1. Synthesis of silver nanoparticles

$AgNO_3$ (1 mM) is dissolved in distilled water. On addition of PLL (0.35 ml) into it, color of the solution is changed from colorless to yellow. Stir the solution for 10 min at 70 °C. Then, CTAB (0.25 mM) is added into the above stirred solution. Final pH of solution is 6.3. The initial color of the solution is changed from yellow to brown within 3 h without any suspension. After 3 h, the sample is cooled to room temperature and kept overnight. Purification of the sample is done with pure water at least two times to remove unreacted PLL and CTAB. AgNPs are centrifuged at 14,000 rpm for 5 min. AgNPs are collected after washing each time with distilled water. Series of reactions have been carried out by varying the concentration of reactant precursor such as $[AgNO_3]$ = 0.5 mM, 1 mM, 2 mM; [PLL] = 0.26 ml, 0.35 ml, 0.44 ml and [CTAB] = 0.2 mM, 0.25 mM, 0.3 mM.

4. Methods

4.1. Spectroscopic and microscopic analysis

UV–Visible measurements are used to understand the reaction kinetics. The optical properties of colloidal AgNPs solution are monitored on Hitachi Model No. U-3900, double beam operated at resolution of 1 nm with spectra range of 200–800 nm using 1 cm path length quartz cuvette. For temperature controlled studies in UV–Visible at constant temperature with in ±10 °C, instrument is equipped with a TCC 240A thermoelectrically temperature controlled cell holder. FTIR spectra of samples in the form of KBr pallets are recorded on Perkin Elmer spectrometer with 1 cm^{-1} resolution and scan range of 4000 cm^{-1} to 400 cm^{-1}. For TEM analysis, samples are prepared by placing drop of sample solution on carbon coated copper TEM grid. The grid is allowed to dry prior to the measurements. TEM measurements are performed on JEOL2010F at an operating voltage of 200 kV. Panalytical'sX'Pert Pro is used for XRD studies of sample. The samples are taken on a glass slide and nickel-filtered CuKα radiation is used to record the diffractogram at a scanning rate of 0.6 degree 2 theta per min.

4.2. Metal ion detection assay

All the analytical studies are performed at 25 ± 1 °C. A sufficient time is given to ensure the uniformity of the solution before recording any spectrum. The cation recognition behavior of PL-CT-AgNPs is evaluated from the changes in UV–Visible absorption upon addition of the metal salt to it in aqueous medium. For titrations, volumetric flasks are taken, each containing a standard solution of PL-CT-AgNPs (2.5 ml of 1 mM) along with various amounts of a different metal salt, 0–200 μM in drinking water and 0–50 μM in polluted river water.

5. Computational analysis

5.1. Results and discussion

We have used the simulation method based on DFT to study the interaction between AgNPs and PLL. A cage like hollow cluster of the silver (Ag) atoms (32 atoms, Fig. SI-2a) has been used to perform first-principles calculations. This cluster has been used because of its high stability and exceptional reactivity [highest occupied molecular orbital (HOMO)-lowest unoccupied molecular orbital (LUMO) gap of the Ag32 cluster is equal to 1.62 eV] and has been previously reported in the literature to model the AgNPs [29,30]. We are primarily interested in how PLL attach on the AgNPs using first principles calculations. In order to model the structure of PLL, we have selected two molecules

of lysine with structure as shown in (Fig. SI-2b). The carboxyl and the amino groups of the lysine interact with each other to form the peptide bond. We have considered the interaction of PLL from different sides with Ag cluster. We come to conclusion that PLL has NH_2 as energetically favorable way of interacting with AgNPs. The Binding energy (BE) comes out to be −0.75 eV. Nitrogen atoms prefer to be on top site, the distance between N (-NH_2) and the Ag atom is about 2.38 Å (Fig. SI-3). In order to analyze the reasons for the affinity of the PLL with the AgNPs, we analyzed the molecular orbitals of the interacting system at different energies. Starting from below the HOMO, we have found the bonding orbital of π-like nature (Fig. 1a).Starting above from the LUMO, antibonding orbital of π-like nature can be observed (Fig. 1b).

It is clear from the molecular orbitals analysis that orbitals associated with the Ag atoms appear in the low-lying LUMO whereas HOMO is localized on PLL (Fig. SI-4a and 4b). The PLL shows signs of the chemisorption at the silver surface, giving rise to the bonding and antibonding like orbitals below and above the d band of the metal as per the Newns-Anderson model (Fig. SI-4c). This model explains that d electron band of the metal interacts with the electron level of the highest occupied state of the adsorbate and it leads to the formation of bonding and antibonding states. Charge density difference plots of the PLL adsorbed on the Ag surface is presented in (Fig. 2). The slices of the charge density difference are obtained by subtracting the charge density of the Ag cluster and the PLL from the relaxed structure of the Ag/PLL. Region of accumulation of charge is seen near to the Ag atom whereas there is region
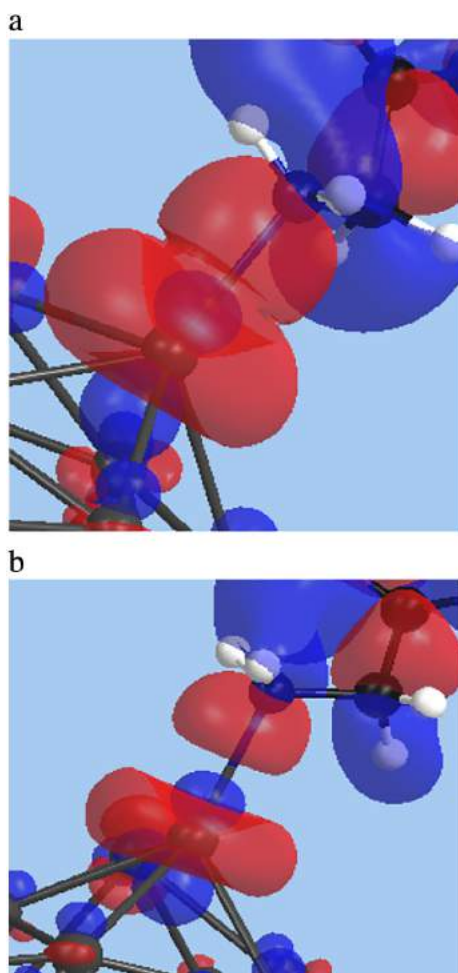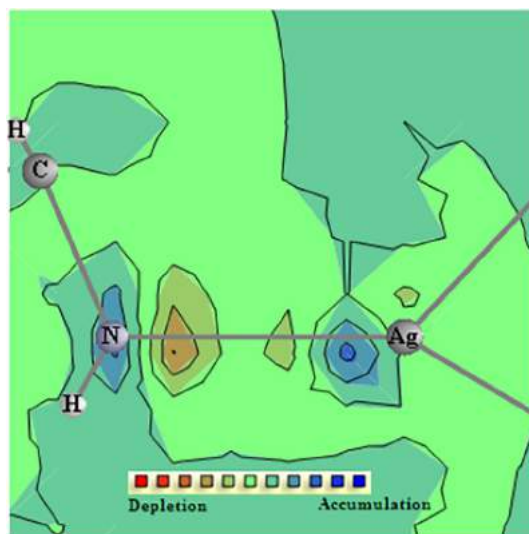

Fig. 2. Charge density difference plot of PLL adsorbed on Ag32 cluster. The slices are taken along the N—Ag bond.

of depletion of charge near the N atom. The region of accumulation and depletions are seen along the direction of the bond. Lowdin charge analysis for the complex also shows that there is a charge transfer from N atom to the Ag cluster (Table 1). Thus, both covalent and ionic interactions contribute towards the enhanced affinity of PLL towards the Ag cluster.

We have also studied the interactions of the CTAB from theoretical perspectives (Fig. SI-5). We have searched out the energy minimum structure of CTAB with Ag cluster starting from two configurations of CTAB. The two configurations of CTAB which can have.

appreciable interactions are its head and tail. The head configuration of CTAB has a BE of −0.44 eV and tail configuration has a BE of −0.006 eV. The value of the BE indicates that head side of the CTAB interacts more favorably with the Ag cluster. The geometry of the minimum energy structure of CTAB head and tail configuration on Ag cluster is shown in Fig. SI-6a and b, respectively. Head of the CTAB is adsorbed to Ag cluster through bond between H and Ag with a bond length equal to 2.5 A°. For structure, where the H atom of head interacts with the Ag atom of the cluster, the charge density difference map is

Fig. 1. Isosurfaces plots for the Ag32/PLL (a) Bonding orbital with π-like shape (b) Antibonding orbital with π-like shape.

Table 1
Calculated Lowdin charges of PLL adsorbed on Ag32 cluster.

Atom	Net Charge
Ag(interacting atom of cluster)	−0.15
N (interacting atom of the PLL)	0.14
C	0.02
C	0.02
O	0.01
H	0.05
H	0.04
H	0.02
H	0.03
N	0.02
C	0
C	0.01
O	0
O	0
H	0
H	0
H	0.01
H	0
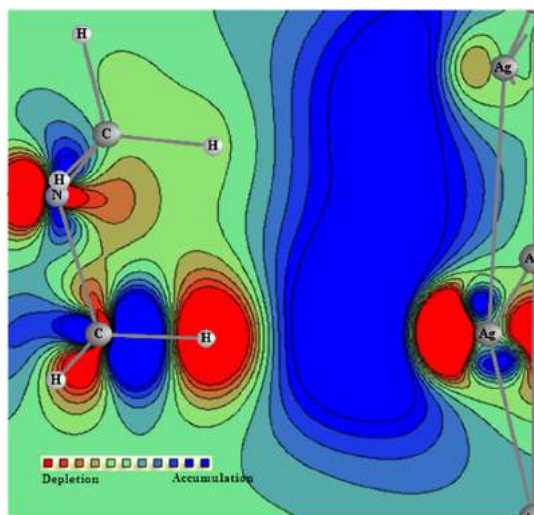
Fig. 3. Charge density difference plot of CTAB adsorbed on Ag32 cluster. The slices are taken along H—Ag bond.

Fig. 4. The charge density difference plot along the line for two possible ways of interacting (a) $Hg(NO_3)_2$ with O atom of PLL (b) $Hg(NO_3)_2$ with Ag32 cluster.

taken along the H—Ag bond (Fig. 3).Along the direction of the H—Ag bond, there is a region of charge depletion around the H atom followed by accumulation of charge between the two atoms and depletion of charge around the Ag atom. It is evident that charge accumulation between the two atoms is symmetric, which shows the signs of the covalent bond between CTAB and the Ag cluster.

In order to analyze the sensing mechanism of Hg^{2+} with the AgNPs, we have relaxed the structure of $Hg(NO_3)_2$ (Fig. SI-7a), this represents our metal salt. We have studied its interaction in two ways [$Hg(NO_3)_2$ can interact with synthesized PL-CT-AgNPs either through PLL or directly with Ag atoms]. In the first case we have carried out the relaxation of $Hg(NO_3)_2$ with PLL, BE after energy minimization comes out to be −0.89 eV. Relaxed structure is shown in Fig. SI-7b. In the second case, we have carried the adsorption of $Hg(NO_3)_2$ with Ag cluster. The Hg ions have high BE in the second case −1.78 eV (Fig. SI-7c). BE is two times higher in the latter case. In order to analyze the cause, we have plotted the charge density difference plots along the line for the two possible ways of interacting $Hg(NO_3)_2$ (Fig. 4a &b). In the case of interactions of $Hg(NO_3)_2$ with PLL, we found that Hg ion forms bond with O atom of PLL. As can be seen from the Fig. 4a that charge transferred from O atom is only 0.5, which is not sufficient to reduce the Hg ion. However, when preferable mode of relaxation of $Hg(NO_3)_2$ is with Ag cluster, then Hg atom forms bond with nearby Ag atoms (Hg tend to form two short and two long bonds with Ag atoms). It nearly transfers a charge equal to 1 electron from two nearest Ag atoms. Hence, it has high probability of getting reduced when it make bond with Ag atom. Mechanism of sensing would have been aggregation if it would have high BE with PLL. It can be concluded that BE of $Hg(NO_3)_2$ with Ag cluster is high, thus, the system is highly selective even in the presence of other metal salts.

6. Experimental results

AgNPs are formed on the addition of PLL to $AgNO_3$. It is confirmed from the change in color of the solution from colorless to turbid brown with suspension, which is also supported from broad SPR band in UV–Visible spectra (Fig. SI-8a). SPR band originates due to collective oscillations of electrons owing to their interaction with incident electromagnetic radiations [31], thus, SPR band of nanosized Ag particles indicate absorbance in UV–Visible region at 420 nm [32]. The quality of NPs can be estimated from the pattern of absorbance peak. Sharp peak indicate small size NPs having narrow size distribution though the broader peak represent the NPs with wide size distribution [33]. Thus, in the
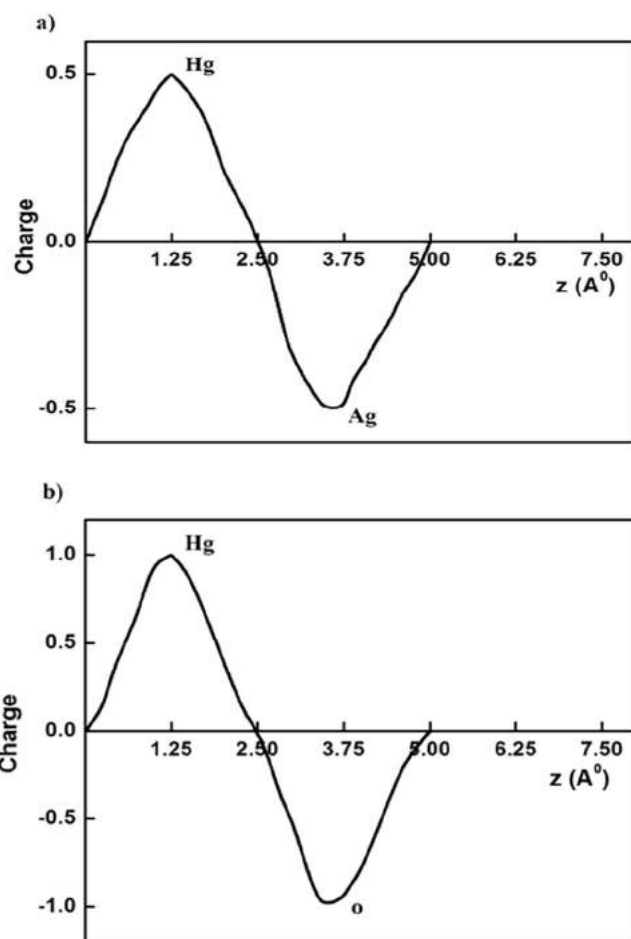
present study, the stability of AgNPs is determined by using CTAB. Reduction of $AgNO_3$ using PLL in the presence of CTAB is carried out at a temperature ranging from 20 °C to 70 °C (Fig. 5a). Aqueous PLL in the presence of CTAB remains in the native state upto 40 °C. Further increase in temperature from 50 °C to 60 °C results in the appearance of a peak at λ_{max} = 450 nm, indicating the presence of AgNPs. Here, 70 °C is considered to be the suitable temperature, where PLL shows its maximum reduction potential in the presence of CTAB. The absorbance around λ_{max} = 450 nm becomes prominent only around this temperature. Therefore, in order to understand the whole mechanism, set of reactions have been carried out by varying the concentration of PLL, CTAB and $AgNO_3$ at 70 °C.

6.1. Effect of concentration of CTAB on AgNPs synthesis

The concentration of [CTAB] = 0.2 mM, 0.25 mM and 0.3 mM is varied by keeping [$AgNO_3$] = 1 mM and [PLL] = 0.35 ml to be constant. At [CTAB] = 0.20 mM (Fig. SI-8b), solution is brown indicating the formation of AgNPs. However, suspension appears after 5 h. At [CTAB] = 0.25 mM (Fig. 5b), the color of the solution remains brown, which is stable with no suspension. At [CTAB] = 0.30 mM (not shown), brown color with suspension appears in 3 h of reaction. In UV–Visible plots of absorbance vs. wavelength, the absorbance increases while wavelength decreases as λ_{max} = 461 nm, 450 nm and 435 nm with increase in the concentration of [CTAB] = 0.2 mM, 0.25 mM and 0.3 mM, respectively.

Plot of intensity at λ_{max} = 460 nm versus time (Fig. 5c) indicates the effect of different concentration of CTAB on the fabrication of AgNPs
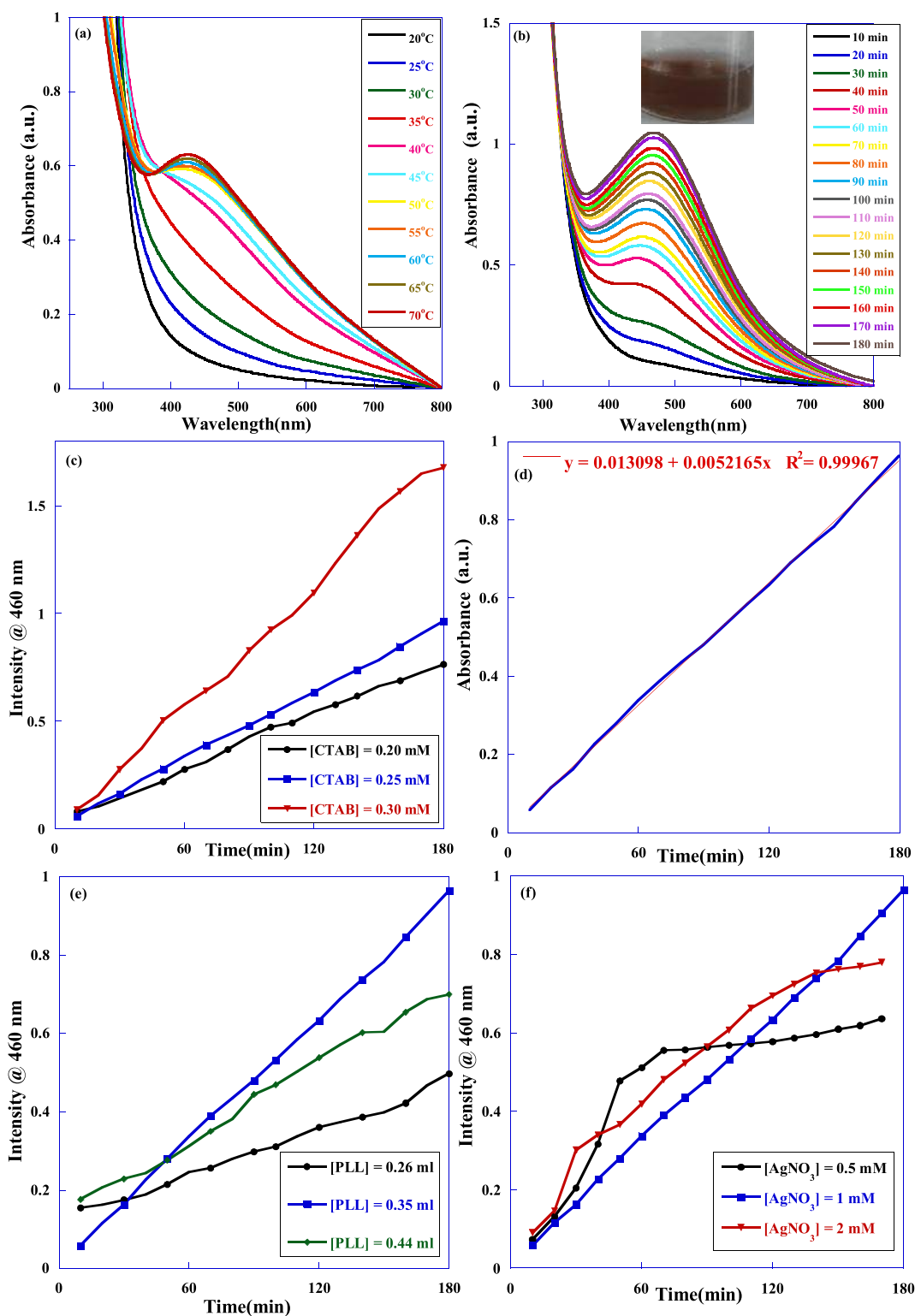
Fig. 5. (a)Absorbance versus wavelength scan of $[AgNO_3] = 1$ mM; $[PLL] = 0.35$ ml; $[CTAB] = 0.25$ mM with respect to reaction temperature from 20 °C to 70 °C (b) UV–Visible spectra of $AgNO_3 + PLL + CTAB$ mixture at 70 °C with $[AgNO_3] = 1$ mM; $[PLL] = 0.35$ ml and $[CTAB] = 0.25$ mM (c) intensity @ 460 nm versus reaction time, respectively for different mixtures keeping $[AgNO_3] = 1$ mM; $[PLL] = 0.35$ ml to be constant and $[CTAB] = 0.20$ mM, 0.25 mM, 0.30 mM. Similarly plots of (d) Absorbance versus time plot for $[AgNO_3] = 1$ mM; $[PLL] = 0.35$ ml; $[CTAB] = 0.25$ mM by selecting maximum points to find linear regression coefficient (e) Intensity @ 460 nm versus reaction time, respectively for different mixtures keeping $[AgNO_3] = 1$ mM; $[CTAB] = 0.25$ mM to be constant and $[PLL] = 0.26$ ml, 0.35 ml, 0.44 ml (f) Intensity @ 460 nm versus reaction time, respectively for different mixtures keeping $[CTAB] = 0.25$ mM; $[PLL] = 0.35$ ml to be constant and $[AgNO_3] = 0.5$ mM, 1 mM, 2 mM.

using PLL at constant temperature. The greater magnitude of the curve is in line with the greater number density of NPs produced. PLL-AgNPs (Inset, Fig. SI-8a) has much lower magnitude of SPR band in comparison

to that in the presence of CTAB. It signifies that the reduction is expedited in the presence of CTAB and least in its absence, i.e. in aqueous PLL only. Moreover, magnitude of the curve increases with an increase

in the concentration of CTAB from 0.2 mM to 0.3 mM. We consider [CTAB] = 0.25 mM to be the best concentration, where AgNPs are the most stable without aggregation. However, at [CTAB] = 0.3 mM plot, there is increase in intensity with time, which is attributed not only to greater number density of AgNPs but a secondary process of complexation of PLL and CTAB might takes place. As a result, a blank experiment to determine the complexation between PLL and CTAB has been carried out (Fig. SI-8c). PLL and CTAB show an edge around 215 nm each, whose intensity increases on mixing both of them. An increased intensity is related to the formation of complex between PLL and CTAB. Thus, at [CTAB] = 0.25 mM, the amount of CTAB is sufficient to stabilize AgNPs, however at [CTAB] = 0.3 mM, CTAB not only stabilize AgNPs but also form a complex with PLL, as a result SPR band becomes flat with increased intensity. It could be further explained in a way as PLL shows different conformation in aqueous solution above 40 °C [34,35]. The dominant conformation of PLL is random coil due to repulsion among protonated lysine residues. However, in our case, 0.1% PLL in water, PLL undergoes acid-base equilibrium as

$$NH_3^+ + H_2O \rightarrow NH_2 + H_3O^+$$
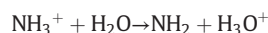
Deprotonated NH_2 allows the existence of alpha helix structure. However, β-sheet structure appears above 40 °C, in which NH_2 sites are available to interact with Ag(I). As a result PLL act as a reducing agent, hence SPR band starts appearing indicating the formation of Ag (0). Now, as the concentration of CTAB increases, it interacts with the adsorbed PLL tails, leading to the conformational changes in the adsorbed polymer. Moreover, more and more CTAB molecules and micelles go into folded chains that stretch more loops further. The stretching is expected to continue until the coils are saturated with adsorbed CTAB micelles and molecules. The conformational changes are based on the ion pair formation between electron pair of NH_2 and positively charged head group of CTAB molecules, which brings a positively charged trimethylammonium group in the vicinity of AgNPs. The mechanism is also illustrated in Scheme 1.

First order rate constant values are 4.14×10^{-3} s^{-1}, 5.21×10^{-3} s^{-1}, 9.79×10^{-3} s^{-1} for [CTAB] = 0.2 mM, 0.25 mM, 0.3 mM. These are calculated by choosing maximum points from the data. The plot with maximum points for [CTAB] = 0.25 mM with linear regression coefficient R^2 = 0.99967 is shown in Fig. 5d.

## 6.2. Effect of concentration of PLL on AgNPs synthesis

To determine the effect of PLL on AgNPs synthesis, UV–Visible plots of wavelength vs absorbance are taken at different amounts of PLL = 0.26 ml, 0.35 ml, 0.44 ml keeping [AgNO$_3$] = 1 mM and [CTAB] = 0.25 mM to be constant. The solution becomes muddy brown with suspension within 3 h at [PLL] = 0.26 ml (Fig. SI-8d) and 0.44 ml (Figure not shown). At [PLL] = 0.35 ml (Fig. 5b), solution turns to brown having λ_{max} = 450 nm with no suspension. Thus, adsorption of PLL along with CTAB at a particular concentration leads to the stabilization of AgNPs.

Intensity @ 460 nm vs time is plotted as shown in Fig. 5e. Intensity increases from PLL = 0.26 ml to 0.35 ml, which directly indicates the greater number of AgNPs formed. Moreover, at PLL = 0.44 ml, magnitude of the intensity again decreases and peak become flattened. Thus, an increase in intensity at PLL = 0.35 ml is related to the facilitation of reduction of Ag(I) to Ag(0). In each case, synthesis of AgNPs begins within 5 min of the reaction time, thus depicting the maximum reduction potential of PLL. First order rate constant values are 1.9 $\times 10^{-3}$ s^{-1}, 5.21×10^{-3} s^{-1}, 3.31×10^{-3} s^{-1} for [PLL] = 0.26 ml, 0.35 ml, 0.44 ml, respectively. The plot with maximum points for [PLL] = 0.35 ml with linear regression coefficient R^2 = 0.99967 is shown in Fig. 5d. These values support that PLL = 0.35 ml is the most suitable amount for the reduction of Ag(I) to Ag(0) along with CTAB.

6.3. Effect of concentration of AgNO$_3$ on AgNPs synthesis

For this, we have taken different concentration of [AgNO$_3$] = 0.5 mM, 1 mM, 2 mM keeping [PLL] = 0.35 ml and [CTAB] = 0.25 mM to be constant. UV–Visible plots at all concentrations have been taken. At [AgNO$_3$] = 0.5 mM (Fig. SI-8e) solution has light brown color with suspension and at higher concentration i.e. [AgNO$_3$] = 2 mM solution has brown color with suspension within 3 h of reaction. [AgNO$_3$] = 1 mM (Fig. 5b) is the most suitable concentration with brown color and no suspension.

Intensity @ 460 nm vs time is plotted as shown in Fig. 5f. Intensity increases from [AgNO$_3$] = 0.5 mM to 1 mM, which directly indicates the greater number of AgNPs formed. Moreover, at [AgNO$_3$] = 2 mM, magnitude of the intensity again decreases. Thus, an increase in intensity at [AgNO$_3$] = 1 mM indicates that it is the most appropriate concentration for the reduction of Ag(I) to Ag(0) in the presence of PLL and CTAB. First order rate constant values are calculated and are 0.9 $\times 10^{-3}$ s^{-1}, 5.21×10^{-3} s^{-1}, 4.32×10^{-3} s^{-1} for [AgNO$_3$] = 0.5 mM,
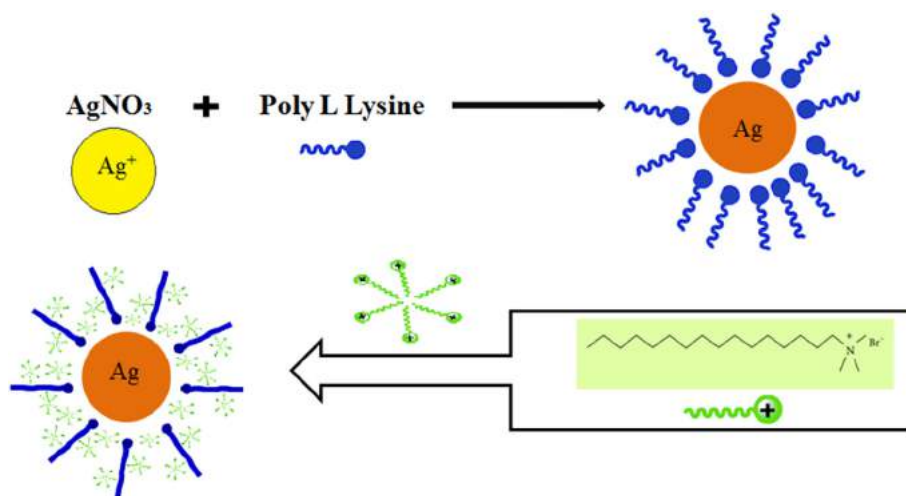
Scheme 1. A schematic illustration of the fabrication process of PL-CT-AgNPs.
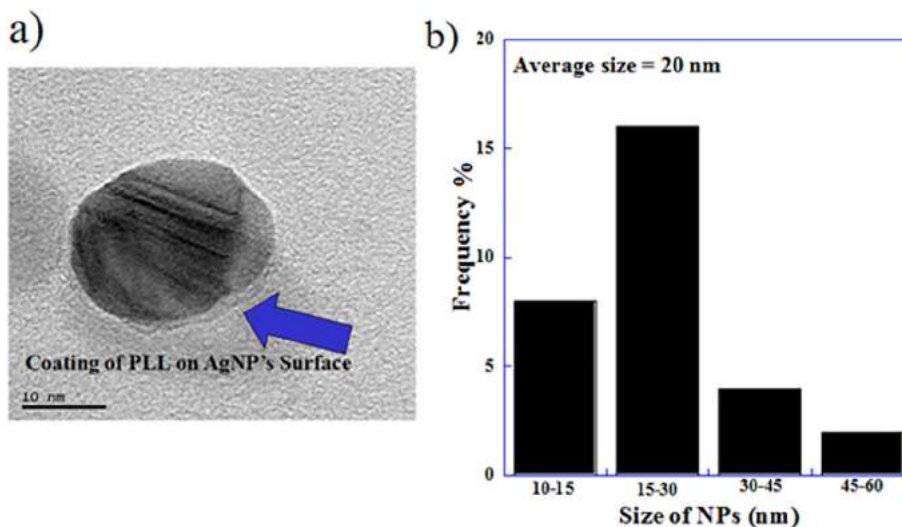
Fig. 6. TEM image of PL-CT-AgNPs. Blue arrow shows a thin layer coating of PLL around each NP. The scale bar corresponds to 10 nm (b) Bar graph showing corresponding particle size distribution of PL-CT-AgNPs.

1 mM, 2 mM, respectively. The plot with maximum points for [AgNO₃] = 1 mM with linear regression coefficient $R^2 = 0.99967$ is shown in Fig. 5d. The rate constant values for different concentrations of CTAB, PLL and AgNO₃ calculated from the plots further support the results. The contour of the curve in each case (Fig. 5c, Fig. 5e and Fig. 5f) exhibits the nature of reaction kinetics. The plots of absorbance versus time clearly indicate that the formation of silver sol has an induction period (nucleation) followed by autocatalysis (growth). Nucleating centers thus created undergo an instant growth process, which is indicated by sharp rise in absorbance in all plots.

6.4. TEM and XRD

The morphology and size of AgNPs prepared using PLL and CTAB is determined from TEM analysis. The TEM images revealed the formation of spherical particles with a thin and tight layer of PLL coated over it, denoted by an arrow in Fig. 6a. The size distribution histogram reveals the average particle size to be 20 nm for PL-CT-AgNPs (Fig. 6b).

The XRD patterns of as formulated PL-CT-AgNPs are shown in Fig. SI-9, revealing the crystalline phases of NPs. The peaks at $2\Theta = 38.3, 44.6, 64.7$ and 77.5 are indexed as planes for AgNPs. The results are to be consistent well with the reported standards (JCPDS file no. 04–0784).

7. Metal ion recognition ability of PLL-AgNPs

PL-CT-AgNPs in the present study is probed for their usage as a colorimetric sensor for the detection of metal ions. The metal ions detection ability of PL-CT-AgNPs is studied for each of the metal ions separately comprising Al(III), Cr(III), Hg(II), Sr(II), Ca(II), Zn(II), Ni(II), Cu(II), Cd(II), Co(II), Mg(II), Mn(II) and Ag(I) at a fixed concentrations of 200 μM. The variation in intensity of absorbance is examined using UV–Visible spectroscopy as shown in Fig. SI-10a. The intensity of the SPR band and color of the solution does not show any significant change upon addition of various metal salts to PL-CT-AgNPs solution. However, upon addition of Hg^{2+}, the color of the solution changed from brown to colorless. Thus, a significant decrease in the intensity of SPR band is observed demonstrating the high sensitivity of PL-CT-AgNPs towards Hg^{2+}. The change in absorption intensity after the addition of different metal ions to the PL-CT-AgNPs solution is demonstrated in Fig. 7a.

To further investigate the ability of Hg^{2+} ions to bind with PL-CT-AgNPs, titration is performed by adding small aliquots of Hg^{2+} to AgNPs

under the similar laboratory conditions. The successive addition of Hg^{2+} (from 0 μM to 200 μM) to PL-CT-AgNPs is shown in (Fig. SI-10b) in which the SPR band of the system is examined with UV–Visible spectroscopy. Fig. SI-10b demonstrates the gradual hypochromic effect in its SPR band upon addition of Hg^{2+} ions to PL-CT-AgNPs solution. The decrease in intensity depends upon the concentration of Hg^{2+} ions in the solution. This could be attributed to a direct redox reaction between zero valent Ag and Hg^{2+} ions, where AgNPs are oxidized to form Ag^+ and Hg^{2+} ions are reduced to Hg, moving away the coating of PLL and CTAB from the surface of AgNPs. It is attributed to the differences in the standard potential of 0.8 V (Ag^+/Ag) and 0.85 V (Hg^{2+}/Hg) [36]. The absorption intensity decreased with increased concentration of Hg^{2+} ions ranging from 0 to 200 μM. The value of linear regression coefficient (R^2) is found to be 0.9999 with the detection limit up to 43 μM (inset, Fig. SI-10b).

To investigate the selectivity of PL-CT-AgNPs for Hg^{2+} ions, competitive metal binding experiments are also performed, to estimate Hg^{2+} in the presence of Cr^{3+}, Cd^{3+}, Cu^{3+}, Co^{3+}, Zn^{2+}, Sr^{2+}, Mg^{2+}, Al^{3+}, Mn^{2+}, Ca^{2+} Ag^{1+} and Ni^{2+}. For this, aqueous solution of Hg^{2+} and other metal ions having concentration 100 μM each is spiked into aqueous solution of PL-CT-AgNPs. There is no change in the absorbance of Hg^{2+} - PL-CT-AgNPs solution on addition of other metal ions (Fig. 7b). Thus, the results indicate that PL-CT-AgNPs possesses good selectivity towards Hg^{2+} in the presence of other metal ions.

7.1. Practical application

The colorimetric response of as synthesized PL-CT-AgNPs towards heavy metal ions is verified in real samples such as in polluted river water. The competency of NPs to detect these metal ions present in the water samples is analyzed by adding different concentrations of Hg^{2+} to the polluted river water sample. A linear decrease in the absorption intensity of PL-CT-AgNPs at 450 nm is detected on varying the concentration of Hg^{2+} from 0 μM to 50 μM (Fig. 7c). The value of linear regression coefficient (R^2) is obtained to be 0.99790 with the detection limit up to 5 μM (inset in Fig. 7c).

8. Conclusions

PLL coated AgNPs are synthesized to explore their applicability as colorimetric sensor. The physical aspects vital for an appropriate synthesis of PLL coated AgNPs, which include the use of CTAB as stabilizing
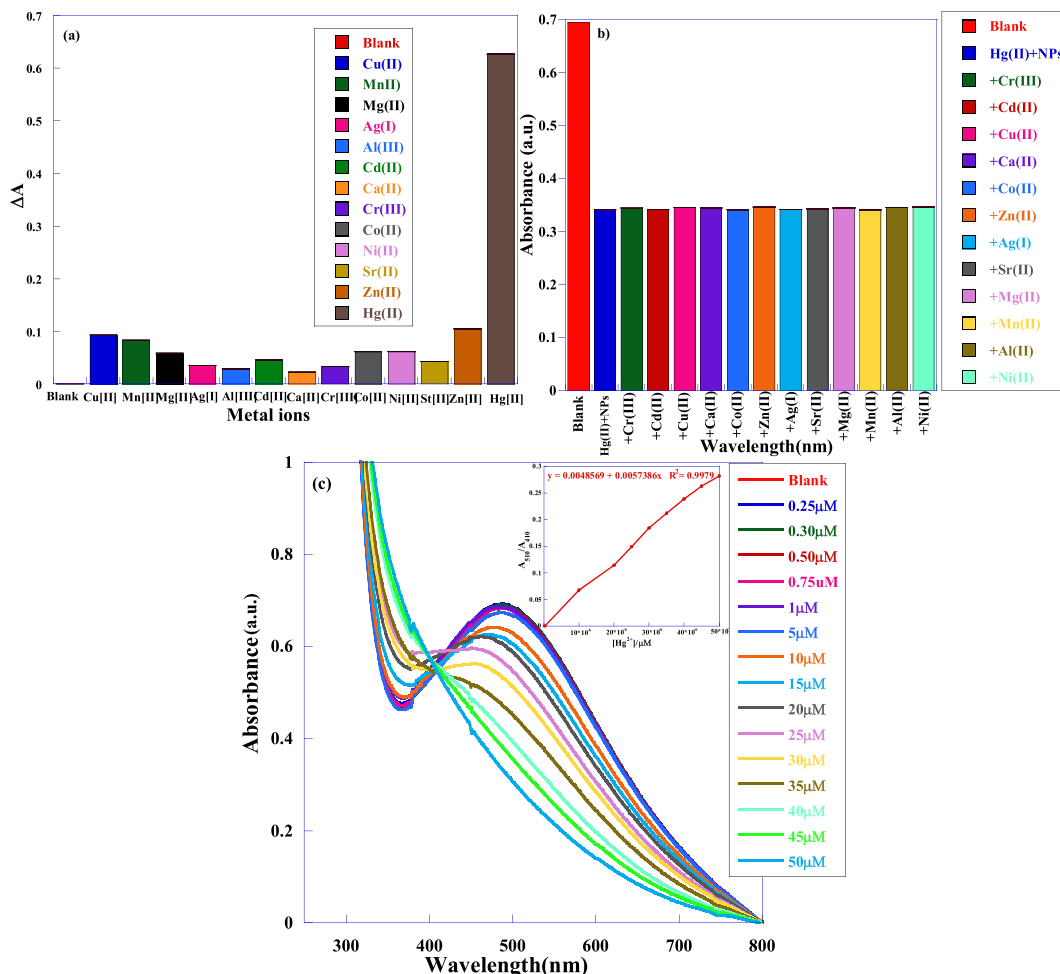
Fig. 7. (a) The bar graph represent the calorimetric response of PL-CT-AgNPs with various metal ions in terms of change in absorbance ΔA with respect to the blank i.e. PL-CT-AgNP (b) The bar graph represent the calorimetric response of PL-CT-AgNPs with mixture of different metal ions in presence of Hg^{2+} in terms of change in absorbance with respect to PL-CT-AgNPs + Hg^{2+} (c) UV–Visible absorbance spectra of PL-CT-AgNPs on addition of $[Hg^{2+}] = 0$ μM to 50 μM in polluted water sample (inset) Plot of absorption ratio of A_{510}/A_{410} of PL-CT-AgNPs vs. versus concentration of Hg^{2+} in polluted water sample.

agent, optimum concentration of PLL and CTAB for the reduction and stability of AgNPs, respectively are also presented. This study demonstrates a strong surface adsorption of PLL and CTAB on AgNPs, which leads the formation of AgNPs best suited for colorimetric sensing of Hg^{2+} ions. Theoretical simulations further support these results. It demonstrates that π-bonding orbitals are responsible for the affinity of PLL to AgNPs. Moreover, there is a charge transfer from PLL (through N of NH_2) to AgNPs. Interaction of CTAB with AgNPs is explained through positively charged trimethylammonium group. There is accumulation of charge between CTAB and Ag atom. DFT studies show that the Hg^{2+} has highest affinity with AgNPs. It draws maximum charge from the two Ag atoms and hence a redox reaction takes place between Ag cluster and the Hg ions.

Appendix A. Supplementary data

Supplementary data to this article can be found online at https://doi.org/10.1016/j.molliq.2018.12.106.

References

[1] F.L. Mi, S.J. Wu, W.Q. Zhong, C.Y. Huang, Preparation of a silver nanoparticle-based dual-functional sensor using a complexation-reduction method, Phys. Chem. Chem. Phys. 17 (2015) 21243–21253.
[2] L.A. Austin, M.A. Mackey, E.C. Dreaden, M.A. El-Sayed, The optical, photothermal, and facile surface chemical properties of gold and silver nanoparticles in biodiagnostics, therapy, and drug delivery, Arch. Toxicol. 88 (2014) 1391–1417.
[3] M. Rani, L. Moudgil, B. Singh, A. Kaushal, A. Mittal, G.S.S. Saini, S.K. Tripathi, G. Singh, A. Kaura, Understanding the mechanism of replacement of citrate from the surface of gold nanoparticles by amino acids: a theoretical and experimental investigation and their biological application, RSC Adv. 6 (2016) 17373–17383.
[4] M.A. Gondal, X. Chang, E.I. Wei, Z.H. Yamani, Q. Zhou, Enhanced photoactivity on Ag/Ag3PO4 composites by plasmonic effect, J. Colloid Interface Sci. 392 (2013) 325–330.
[5] S. Singh, B. Singh, P. Sharma, A. Mittal, S. Kumar, G.S.S. Saini, S.K. Tripathi, G. Singh, A. Kaura, Amino acid functionalized zinc oxide nanostructures for cytotoxicity effect and hemolytic behavior: theoretical and experimental studies, Mater. Des. 134 (2017) 10–22.
[6] P. Khullar, M.K. Goshisht, L. Moudgil, G. Singh, D. Mandial, H. Kumar, G.K. Ahluwalia, M.S. Bakshi, Mode of protein complexes on gold nanoparticles surface: synthesis and characterization of biomaterials for hemocompatibility and preferential DNA complexation, ACS Sustain. Chem. Eng. 5 (2017) 1082–1093.
[7] M.K. Goshisht, L. Moudgil, P. Khullar, G. Singh, A. Kaura, H. Kumar, G. Kaur, M.S. Bakshi, Surface adsorption and molecular modeling of biofunctional gold nanoparticles for systemic circulation and biological sustainability, ACS Sustain. Chem. Eng. 3 (2015) 3175–3187.
[8] S. Gupta, M. Kashyap, V. Kumar, P. Jain, V. Vinayak, K.B. Joshi, Peptide mediated facile fabrication of silver nanoparticles over living diatom surface and its application, J. Mol. Liq. 249 (2018) 600–608.
[9] S.B. Abram, J. Aupic, G. Drazic, H. Gradisar, R. Jerala, Coiled-coil forming peptides for the induction of silver nanoparticles, Biochem. Biophys. Res. Commun. 472 (2016) 566–571.

[10] A. Chandra, M. Singh, Biosynthesis of amino acid functionalized silver nanoparticles for potential catalytic and oxygen sensing applications, Inorg. Chem. Front. 5 (2018) 233–257.

[11] Z. Khan, S.A. Al-Thabaiti, A.Y. Obaid, Z.A. Khan, A.A.O. Al-Youbi, Shape-directing role of cetyltrimethylammonium bromide in the preparation of silver nanoparticles, J. Colloid Interface Sci. 367 (2012) 101–108.

[12] Z. Zaheer, M.A. Malik, F.M. Al-Nowaiser, Z. Khan, Preparation of silver nanoparticles using tryptophan and its formation mechanism, Colloids Surf. B: Biointerfaces 81 (2010) 587–592.

[13] M.N. Khan, O. Bashir, T.A. Khan, S.A. Al-Thabaiti, Z. Khan, CTAB capped synthesis of bio-conjugated silver nanoparticles and their enhanced catalytic activities, J. Mol. Liq. 258 (2018) 133–141.

[14] A. Rafey, K.B.L. Shrivastavaa, S.A. Iqbal, Z. Khan, Growth of Ag-nanoparticles using aspartic acid in aqueous solutions, J. Colloid Interface Sci. 354 (2011) 190–195.

[15] I. Shtepliuk, V. Khranovskyy, R. Yakimova, Insight into the origin of the excited transitions in grapheme quantum dots interacting with heavy metals in different media, Phys. Chem. Chem. Phys. 19 (2017) 30445–30463.

[16] M. Farina, D.S. Avila, J.B.T. da Rocha, M. Aschner, Metals, oxidative stress and neurodegeneration: a focus on Iron, manganese and mercury, Neurochem. Int. 62 (2013) 575–594.

[17] L. Adlnasab, H. Ebrahimzadeh, A.A. Asgharinezhad, M.N. Aghdam, A. Dehghani, S. Esmaeilpour, A preconcentration procedure for determination of ultra-trace mercury (II) in environmental samples employing continuous-flow cold vapor atomic absorption spectrometry, Food Anal. Methods 7 (2014) 616–628.

[18] Y. Gao, Z. Shi, Z. Long, P. Wu, C. Zheng, X. Hou, Determination and speciation of mercury in environmental and biological samples by analytical atomic spectrometry, Microchem. J. 103 (2014) 1–14.

[19] X. Cheng, Y. Yu, Y. Jia, L. Duan, Fluorescent PU films for detection and removal of Hg^{2+}, Cr^{3+} and Fe^{3+} ions, Mater. Des. 95 (2016) 133–140.

[20] Y. Zhou, H. Zhao, C. Li, P. He, W. Peng, L. Yuan, L. Zeng, Y. He, Colorimetric detection of Mn^{2+} using silver nanoparticles cofunctionalized with 4-mercaptobenzoic acid and melamine as a probe, Talanta 97 (2012) 331–335.

[21] K. Farhadi, M. Forough, R. Molaei, S. Hajizadeh, A. Rafipour, Highly selective Hg^{2+} colorimetric sensor using green synthesized and unmodified silver nanoparticles, Sensors Actuators B 161 (2012) 880–885.

[22] Y. Wang, F. Yang, X. Yang, Colorimetric detection of mercury(II) ion using unmodified silver nanoparticles and mercury-specific oligonucleotides, ACS Appl. Mater. Interfaces 2 (2010) 339–342.

[23] M. Annadhasan, T. Muthukumarasamyvel, V.R. SankarBabu, N. Rajendiran, Green synthesized silver and gold nanoparticles for colorimetric detection of Hg^{2+}, Pb^{2+}, and Mn^{2+} in aqueous medium, ACS Sustain. Chem. Eng. 2 (2014) 887–896.

[24] S. Maiti, G. Barman, J.K. Laha, Detection of heavy metals (Cu^{2+}, Hg^{2+}) by biosynthesized silver nanoparticles, Appl. Nanosci. 6 (2016) 529–538.

[25] V.E. Matulis, O.A. Lvashkevich, V.S. Gurin, DFT study of electronic structure and geometry of neutral and anionic silver clusters, J. Mol. Struct. THEOCHEM 664–665 (2003) 291–308.

[26] B. Singh, M. Rani, J. Singh, L. Moudgil, P. Sharma, S. Kumar, G.S.S. Saini, S.K. Tripathi, G. Singh, A. Kaura, Identifying the preferred interaction mode of naringin with gold nanoparticles through experimental, DFT and TDDFT techniques: insights into their sensing and biological applications, RSC Adv. 6 (2016) 79470–79484.

[27] M. Valiev, E.J. Bylaska, N. Govind, K. Kowalski, T.P. Straatsma, H.J.J. Van Dam, D. Wang, J. Nieplocha, E. Apra, T.L. Windus, W.A. de Jong, NWChem: a comprehensive and scalable open-source solution for large scale molecular simulations, Comput. Phys. Commun. 181 (2010) 1477–1489.

[28] L. Skripnikov, A Computer Program to Analyse and Visualise Quantum-chemical Calculations, 2012.

[29] T. Udayabhaskararao, T. Pardeep, New protocols for the synthesis of stable Ag and Au nanocluster molecules, J. Phys. Chem. Lett. 4 (2013) 1553–1564.

[30] T. Udayabhaskararao, M.S. Bootharaju, T. Pardeep, Thiolate-protected Ag_{32} clusters: mass spectral studies of composition and insights into the Ag–thiolate structure from NMR, Nanoscale 5 (2013) 9404–9411.

[31] R. Das, S.S. Nath, D. Chakdar, G. Gope, R. Bhattacharjee, Synnthesis of silver nanoparticles and their optical properties, J. Exp. Nanosci. 5 (2010) 357–362.

[32] E. Filippo, A. Serra, D. Manno, Poly(vinyl alcohol) capped silver nanoparticles as localized surface plasmon resonance-based hydrogen peroxide sensor, Sensors Actuators B 138 (2009) 625–630.

[33] V.S. Jaswal, P.K. Banipal, A. Kaura, M.S. Bakshi, Bovine serum albumin driven interfacial growth of selenium-gold/silver hybrid nanomaterials, J. Nanosci. Nanotechnol. 11 (2011) 3824–3833.

[34] B. Davidson, G.D. Fasman, The conformational transitions of uncharged poly-ʟ-lysin. A helix-random coil-β structure, Biochemistry 6 (1967) 1616–1629.

[35] K. Cieslik-Boczula, Alpha-helix to beta-sheet transition long-chain poly-ʟ-lysine: formation of alpha of alpha-helical fibrils by poly-ʟ-lysine, Biochimie 137 (2017) 106–114.

[36] P. Rameshkumar, S. Manivannan, R. Ramaraj, Silver nanoparticles deposited on amine-functionalized silica spheres and their amalgamation-based spectral and colorimetric detection of Hg(II) ions, J. Nanopart. Res. 15 (2013) 1–9.